Reluctance Synchronous and Field Intensified-PM Motors for Variable-Gear Electric Vehicle Drives

Michiel H.A. Prins, Chris W. Vorster and Maarten J. Kamper, SMIEEE
Department of Electrical and Electronic Engineering
Stellenbosch University, Stellenbosch, South-Africa
Email: kamper@sun.ac.za

***Abstract*—Reluctance synchronous (RS) and field-intensified permanent magnet (FI-PM) motors are designed and optimised for a variable-gear electric vehicle (EV) drive in this paper. Recent literature shows that EVs with variable-gear drive trains operate at higher drive-cycle efficiencies than fix-gear EV drive trains. The advantages and design challenges of variable-gear EV drives are discussed in the paper. With variable-gear, the operation field-weakening performance of the electric drive is not important, which makes the RS motor drive, amongst others, very suitable. The FI-PM motor with minimum amount of PM material is also attractive from the performance and position-sensorless-control points of view. It is found that both the optimum designed RS and FI-PM motors perform very well considering the volumetric space available and the required torque-speed specifications. In particular, the performance of the FI-PM motor with the same volume as the RS motor is surprising considering the simple FI-PM rotor structure proposed. The variable gear system was tested and the average efficiency was found to above 80%.**

NOMENCLATURE

st_{od}	Stator outer diameter (in mm).
st_{id}	Stator inner diameter (in mm).
ro_{id}	Rotor inner diameter (in mm).
g	Air gap (in mm).
ℓ_s	Axial stack length (in mm).
y_h	Yoke height (in mm).
t_w	Tooth width (in mm).
o_w	Outer width (in mm).
i_w	Inner width (in mm).
$c_{1,..4}$	Centre points 1-4 (in mm).
$\varphi_{1,..4}$	Angles 1-4 (in mechanical degrees).
x_p	Point on x-axis (in mm).
m_w	Magnet width (in mm).
m_h	Magnet height (in mm).
$p_{1,2}$	Pole pitch 1 and 2 (in mm).
$b_{p1,..3}$	Barrier pitches 1-3 (in mechanical degrees).
$b_{w1,..3}$	Barrier widths 1-3 (in mm).

I. INTRODUCTION

Hybrid and pure battery-powered electric vehicles (EVs) are considered more and more often by industry today. In the spectrum of EV drives, research focuses on direct in-wheel(hub) drives on the one side to fixed-gear (FG) plus differential single-electric motor drives on the other side of the spectrum. A further step in this spectrum is to use the variable-gear (VG) plus differential electric drive train, similar to what is used in internal combustion engine (ICE) powered vehicles. The ideal torque-speed characteristics of the VG ICE powered vehicle, as shown by the dotted lines in Fig. 1, match perfectly with the torque-speed characteristics of a FG electric motor drive system in field weakening mode [1], [2].

Hence, single electric motor EV drives are usually implemented with FG transmissions. With FG EV drives the power performance of the vehicle strongly depends on the field weakening performance or the constant power speed range (CPSR) of the electric drive. The control strategy for these types of EV motor drives sometimes requires a fairly complex field-weakening operation of the electric motor in order to achieve acceptable power and efficiency performance for the vehicle at higher speeds. Furthermore, with a relatively high FG-ratio (to keep the electric motor small), the speed of the drive motor becomes excessively high as is explained in the next section. This, in turn, requires careful consideration of the motor bearings and the core losses in the case of permanent magnet drive motors.
Variable-gear (VG) electric drive trains for EVs receive almost no attention in literature. It is only recently that studies show [2]–[6] that VG EVs operate, surprisingly, more optimally on the drive-cycle efficiency map than FG EVs. This results in an increased vehicle range or a smaller battery pack.

VG EV drives have numerous advantages, amongst others a much smaller traction motor operating at relatively low speeds. The VG EV drive also has the advantage in higher traction applications such as for taxis, buses and agriculture vehicles. The other advantages of VG EV drives are briefly given in the next section. One very important aspect of the VG EV

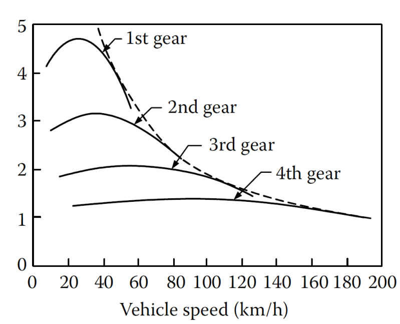

Fig. 1: Torque speed curve of ICE with variable-gear transmission.

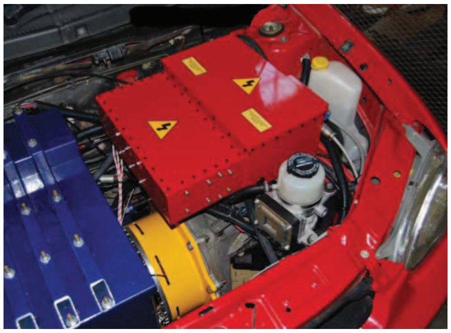

Fig. 2: E-Corsa with traction motor (yellow), inverter (red) and battery pack (blue).

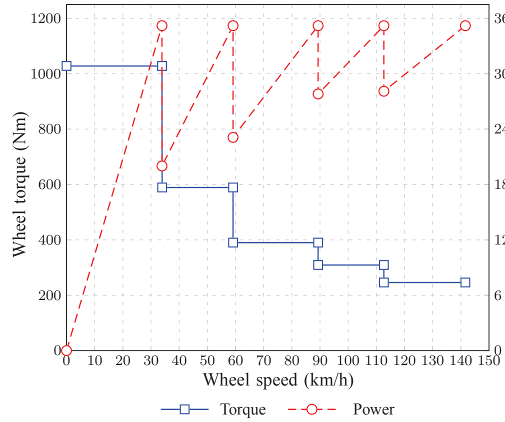

Fig. 4: Tractive effort of the vehicle with 5-speed transmission.

drive is that a good field-weakening performance or large CPSR is no longer a requirement. Hence, drives with a poor field-weakening performance, such as PM brushless DC and the reluctance synchronous (RS) motor drives, can be used. An outstanding feature of the RS motor drive is its higher operating efficiency compared to that of the induction motor drive [7], [8]. RS motor drives, however, have the problem of losing saliency at high loads which are required for position sensorless control - position sensorless control, even for back-up, is a necessity in EV drives. For this reason field-intensified PM (FI-PM) motor drives can be considered [9], [10]. The switched reluctance motor drive is another option for the VG EV drive. In this paper, with the focus on zero or low magnet content in the traction drive motor, the design and performance of RS and FI-PM motors for VG EV drives are considered. As the types of motor used in the investigation of [2]–[6] are not mentioned, this is the first time that RS and FI-PM motors for VG-EV drives have been evaluated and reported on. An Opel Corsa 1.4i Light car with a 5-speed VG is used in the case study. A first iteration is shown in Fig. 2.

II. Variable-Gear EV Drive

A basic diagram of the variable gear electric drive train system used in the Opel Corsa battery powered EV is shown in Fig. 3. In this study the clutch and standard 5-speed manual transmission of the Opel Corsa are used. It must be mentioned that in modern VG single motor EV drives a clutch-system for VG operation is, per se, not necessary as VG operation can be done by proper synchronisation motor control [4]. The proposed RS and FI-PM motor drives for each gear are designed according to the tractive-effort and power specifications of the ICE-powered Opel Corsa as shown in Fig. 4. The reason for this is that with the latest battery technology and battery energy/mass ratio, the overall mass of the battery-powered Opel Corsa is very much the same as that of the ICE-powered Opel Corsa. From Fig. 4 it is evident that the vehicle can ascend a very steep road gradient with the high tractive effort in 1st gear, though maintaining a reasonable top speed in 5th gear. At a top vehicle speed of 140 km/h in 5th gear, an electric traction motor torque of 70 Nm at a motor speed of 4800 r/min (35 kW) is required. The maximum required traction motor torque according to the ICE-specifications, is 110 Nm or 1.57 pu torque. The rated torque-speed characteristic of the electric Opel Corsa VG drive is shown in Fig. 5. Also shown are the torque-speed characteristics of two FG drives with different FG ratios, both satisfying the required vehicle tractive-effort- and power specifications. With a high fix gear ratio of 14.68:1 the traction motor torque and volumetric size are the same as that of the VG traction motor, however, the FG traction motor drive must operate at speeds above 20 000 r/min at maximum vehicle speed.

With the FG ratio halved to 7.34:1, the maximum speed is also halved to 10 000 r/min, but the volumetric size of the

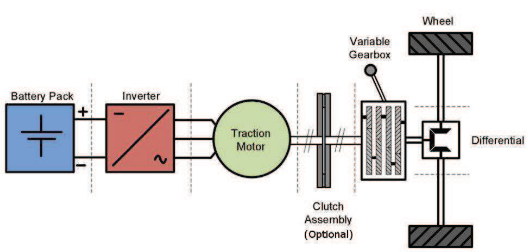

Fig. 3: Layout of the variable-gear EV drive train.

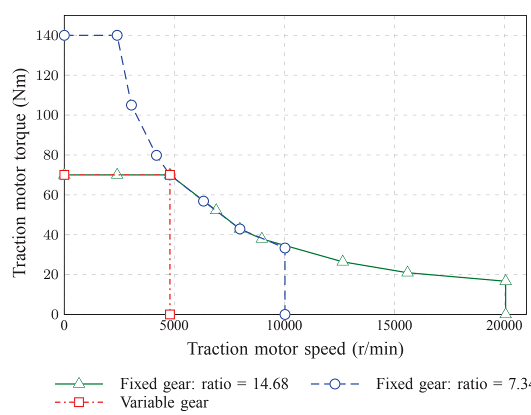

Fig. 5: Torque-speed graphs for different fixed-gear ratios.

traction motor more or less doubles due to the double torque required. This much larger motor must also be designed to operate at double the maximum speed of the VG motor option. The FG traction motor, thus, has a cost and efficiency implication. One disadvantage of the VG drive is that a constant (rated) wheel power versus vehicle speed cannot be obtained at rated torque as shown in Fig. 4, but all required wheel torques can be obtained. VG transmissions offer some benefits over FG transmissions. VG transmission technology is very well developed today. These transmissions are efficient, cheap and reliable since they have been in mass production for long time. Furthermore the lower gear of the VG transmission can be selected for maximum tractive-effort braking and neutral can be selected for safe towing.

III. E-Corsa Drive Specification

The design specifications of the RS and FI-PM motors as given in Table I are based on the ICE specifications and gearbox dimensions of the Opel Corsa vehicle. Because the motors have to fit on the bell-housing of the gearbox, the maximum available outer diameter for the stator is 230 mm.

The cross-sections of the evaluated RS and FI-PM motors are shown in Fig. 6a and Fig. 6b respectively. The motors are 4-pole motors with 36-slot stators. At a speed of 4800 r/min the operating frequency for the 4-pole motors is 160 Hz. The axial length of the motor stack is a variable in the design.

TABLE I: Specification of the RS and FI-PM motors

Specification	Value	Unit
Rated torque	70	Nm
Rated power	35	kW
Peak torque	110	Nm
Peak power	55	kW
Maximum speed	4800	r/min
Battery pack voltage	350	V
Stator outer diameter	230	mm
Shaft diameter	43	mm
Air-gap length	0.4	mm
Number of poles	4	
Cooling	air	

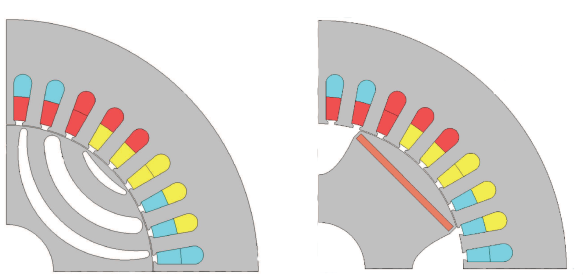

(a) (b)

Fig. 6: Quarter cross-sections of (a) RS and (b) FI-PM motors

IV. Performance Calculations

Finite element (FE) analysis, amongst others, is used to calculate the performance parameters of the motors necessary for the design optimization. In the FE simulation the rotor is stepped through only one torque periodicity (60° elec) to get accurate detail of the average torque and torque ripple. The average torque is calculated as

$$T_{avg} = \frac{1}{n} \sum_{i=0}^{n} \frac{1}{k_s} \sum_{j=1}^{k_s} \tau\left(\theta_i \pm \alpha_j\right) \quad , \tag{1}$$

where n is the number of position steps, k_s is the number of skewed sub motors and $\tau(\theta \pm \alpha)$ is the FE torque at position θ_i and α_j the skew angle of the sub motor. τ is calculated by the FE program using Maxwell's Stress Tensor method as

$$\tau(\theta_i \pm \alpha_j) = \frac{1}{\mu_0} \oint_{\Gamma} r B_t B_n \cdot d\Gamma \times \ell_s \quad , \tag{2}$$

where μ_0 is the permeability of free space, r is the radius of the contour Γ in the centre of the air-gap, B_t and B_n the normal and tangential flux densities in the air-gap respectively and ℓ_s the stack length. With accurate torque versus position detail available the torque ripple is calculated by

$$T_{ripple} = \left(\frac{T_{max} - T_{min}}{T_{avg}}\right) \quad . \tag{3}$$

The copper loss is calculated in the dq reference frame as

$$P_{cu} = \frac{3}{2}\left(I_d^2 + I_q^2\right) r_{ph} \quad , \tag{4}$$

where $I_d = I_s cos(\delta)$ and $I_q = I_s sin(\delta)$ with δ being the angle of the current space phasor. $r_{ph} = r_{ph(stack)} + r_{ph(end)}$ is the resistance of the winding per phase taking the end winding into account. The fundamental voltage of the motors is calculated in the dq reference frame in the steady state by

$$V_d = r_{ph} I_d - \omega\, \lambda_{q(avg)} \tag{5}$$

and

$$V_q = r_{ph} I_q + \omega\, \lambda_{d(avg)} \quad , \tag{6}$$

where $\lambda_{d(avg)}$ and $\lambda_{q(avg)}$ are the average d and q flux linkages and ω the electrical angular speed. For the FI-PM motor the permanent magnet flux linkage component is included in $\lambda_{d(avg)}$ of (6), with the d-axis in this case aligned with the permanent magnet.

The core losses are not taken into account in the design optimization as it is relatively small compared to the copper loss for the evaluated motors. The core losses, however, are an important factor due to the high operating frequency at full flux, but can be limited by using thin high frequency lamination steel for the stator, e.g. NO20 steel. The core losses, hence, are only calculated after the design optimization to check whether they are acceptable and also to calculate the motor's efficiency.

To get an accurate estimate of the core losses from the FE analysis, the motor is stepped through a full electrical period

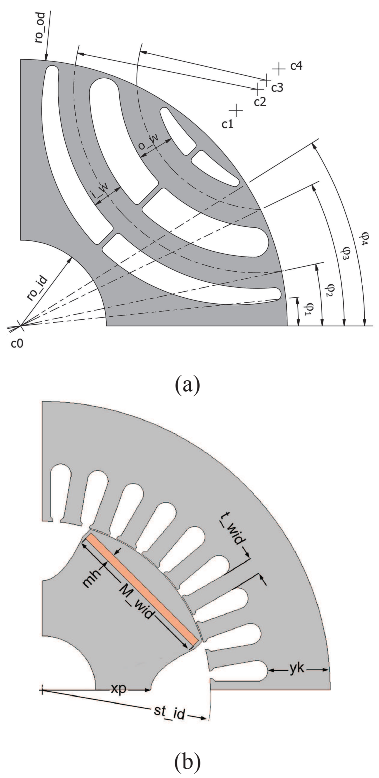

Fig. 7: Design variables of the rotor of (a) the RS motor and the design variables of (b) the FI-PM motor. The RS and the FI-PM motors have the same stator variables.

The specific iron loss consisting of the hysteresis- and eddy current losses are calculated as follows:

Hysteresis loss:

$$P_h = \sum_{e=1}^{E} \left\{ \sum_{k=1}^{N} \alpha\left(|B_k|\right) \cdot f_k \right\} V_e \quad , \tag{7}$$

where α is the coefficient of the magnetic flux density $|B_k|$ for harmonic order k determined by the frequency separation method, f_k is the frequency for harmonic order k, V_e is the volume of each element, N is the maximum frequency order and E is the number of elements.

Eddy current loss:

$$P_e = \sum_{e=1}^{E} \left\{ \sum_{k=1}^{N} \beta\left(|B_k|, f_k\right) \cdot f_k^2 \right\} V_e \quad , \tag{8}$$

where β is the coefficient of the magnetic flux density $|B_k|$ and frequency f_k for harmonic order k determined by the frequency separation method. The iron loss obtained is multiplied by a factor of 20% to account for excess loss [11].

V. Design Optimization of the RS and FI-PM Motors

The design optimization of both RS and FI-PM motors is done by means of the optimization algorithms of the VisualDoc software [12] that are linked by means of a Python script with JMAG's FE simulation program.

A. RS Motor

Due to the complex structure of the RS rotor there are ten design variables on the rotor and three on the stator. The design variables are shown in Fig. 7a. A multi-objective function is used and is given by

$$F(\mathbf{X_1}) = (F_1(\mathbf{X_1}), (F_2(\mathbf{X_1})), \tag{9}$$

where

$$F_1(\mathbf{X_1}) = \frac{Pcu}{T_{avg}}(\mathbf{X_1}) \tag{10}$$

and

$$F_2(\mathbf{X_1}) = T_{ripple}(\mathbf{X_1}) \tag{11}$$

are to minimized, with constant dimensions as

$$\mathbf{U_1} = \begin{bmatrix} st_{od} \\ ro_{id} \\ g \\ \delta \end{bmatrix} = \begin{bmatrix} 230.0 \\ 43.0 \\ 0.4 \\ 67.0 \end{bmatrix}, \tag{12}$$

and $\mathbf{X_1}$ a vector matrix containing the variables as

$$\mathbf{X_1^T} = \begin{bmatrix} t_w & st_{id} & o_w & i_w & c_1 & c_2 & .... \\ .... & c_3 & c_4 & \varphi_1 & \varphi_2 & \varphi_3 & \varphi_4 \end{bmatrix} \tag{13}$$

In the optimization the current density is kept constant and the copper loss is calculated according to (4) for each algorithm iteration. The phase resistance r_{ph} is a function of the slot area. Hence, when the slot area changes the copper loss changes. The optimum current angle δ for maximum torque per ampere at rated current density was found for this specific RS motor to be at around 67°. Therefore in the design optimization δ was chosen as a constant as $\delta = 67°$ as in (12), rather than making it a variable. After the design optimization of the RS motor the stack length is varied to find the required rated torque of $T_{avg} = 70$ Nm at rated current. The rated torque was found with a stack length of $\ell_s = 110$ mm.

B. FI-PM Motor

The FI-PM motor has a very simple rotor structure with only three design variables on the rotor as shown in Fig. 7b. To evaluate the performance of the FI-PM motor the same stator dimensions and stack length of the RS motor are chosen.

The objective function to be minimized in this case is the PM volume expressed as

$$F(\mathbf{X_2}) = V_{PM}(\mathbf{X_2}) \tag{14}$$

subject to the constraint of

$$\mathbf{H_1} = \begin{bmatrix} T_{avg} \end{bmatrix} > \begin{bmatrix} 70.0 \end{bmatrix} \tag{15}$$

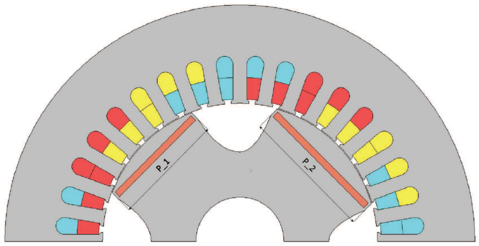

Fig. 8: Half cross-section of Asymmetric FI-PM.

and constants as

$$\mathbf{U_2} = \begin{bmatrix} st_{od} \\ ro_{id} \\ g \\ \ell_s \end{bmatrix} = \begin{bmatrix} 230.0 \\ 43.0 \\ 0.4 \\ 110.0 \end{bmatrix}, \tag{16}$$

where the matrix vector $\mathbf{X_2}$ includes the optimization variables as

$$\mathbf{X_2^T} = \begin{bmatrix} \delta & x_p & m_w & m_h \end{bmatrix}. \tag{17}$$

The same current density as the RS motor is chosen, therefore, since the stator dimensions do not change in this case the copper loss stays constant in the design optimization. The minimum thickness before the PM demagnetizes is found to be 2.5 mm. Due to manufacturing constraints the PM thickness must be $\geq$ 3 mm. Since the torque is a function of the current angle, it is also a variable in the design optimization as given in (17), to ensure the optimum angle for minimum PM volume.

The rotor structure of the FI-PM motor causes a high torque ripple of 39%. The torque ripple can be reduced to an acceptable value by skewing the rotor with a number of stacks. Since the rotor contains PMs, to skew with a number of stacks during the manufacturing process is difficult. A new topology is implemented where the pole widths are asymmetric as shown in Fig. 8.

In a next design optimization of the FI-PM motor the torque ripple is minimized by changing only the two rotor pole widths of Fig. 8. Hence the torque ripple objective function

$$F(\mathbf{X_3}) = T_{ripple}(\mathbf{X_3}) \tag{18}$$

is minimized subject to the constraint of

$$\mathbf{H_2} = \begin{bmatrix} T_{avg} \end{bmatrix} > \begin{bmatrix} 70.0 \end{bmatrix}, \tag{19}$$

and $\mathbf{X_3}$ the vector matrix containing the variables

$$\mathbf{X_3^T} = \begin{bmatrix} p_1 & p_2 \end{bmatrix}. \tag{20}$$

VI. Calculated Performance Results of Optimized Motors

The optimum values of the design variables of $\mathbf{X_1}$, $\mathbf{X_2}$ and $\mathbf{X_3}$ found from the design optimizations are given in Tables II and III. Note from these results, amongst others, the difference in the optimum current angle between the RS and FI-PM motors, and the difference between the pole widths of the asymmetric-rotor FI-PM motor.

TABLE II: Optimum design variables $\mathbf{X_1}$ for RS motor

Variables	y_h	t_w	st_{id}	o_w	i_w
Values	24.67	6.76	143.4	9.16	7.81
Variables	c_1	c_2	c_3	c_4	φ_1
Values	54.03	59.3	61.58	90.94	5.91°
Variables	φ_2	φ_3	φ_4		
Values	11.85°	25.87°	32.14°		

TABLE III: Optimum design variables $\mathbf{X_2}$ and $\mathbf{X_3}$ for FI-PM motor

Variables (X_2)	δ	xp	m_w	m_h
Values	71°	43.457	30.32	3.0
Variables (X_3)	p_1	p_2		
Values	31.35	26.25		

TABLE IV: Performance of RS and FI-PM Motors

Parameters	I_{rms}	V_{rms}	T	T_{ripple}
RSM	$136.23A$	$114.28V$	$68.9N.m$	6.9%
A-FI-IPM	$142.7A$	$119.76V$	$69.3N.m$	6.6%
Parameters	P_{cu}	P_{iron}	P_{rot}	P_{out}
RSM	$1266W$	$435.6W$	$135.2W$	$35.721kW$
A-FI-IPM	$1266W$	$410.3W$	$133.34W$	$35.1kW$
Parameters	η	P_f	CU_{mass}	PM_{volume}
RSM	95.0%	0.71	$8.4kg$	–
A-FI-IPM	94.78%	0.72	$8.4kg$	$80.39cm^3$

The performance parameters of the two motors are given in Table IV for rated torque and maximum speed. Note that all the performance parameters of the two motors are very similar. The iron loss, for both motors, is approximately a third of the copper loss when using the NO20 lamination steel. The efficiencies of both motors are high making them very favourable for EV application. Figs. 9 and 10 shows the efficiency maps of the RS and FI-PM motors respectively. Note that the efficiency increases with speed and current.

The torque of the RS is shown in Fig. 11 and the torque of the FI-PM in Fig. 12. The figures show the rated torque and the maximum torque at 1.57 pu. It is evident that the RS motor has to be skewed to lower the torque ripple while the FI-PM motor has an asymmetric rotor to lower the torque ripple.

A phase voltage of $V_{phase} = 150\,V$ at 160 Hz can be delivered from the battery pack. Both motors are within the working limit of 150 V. The no-load back EMF of the FI-PM motor should not exceed the inverter voltage limit and is found to be 142 V at maximum speed, which is lower than 150 V.

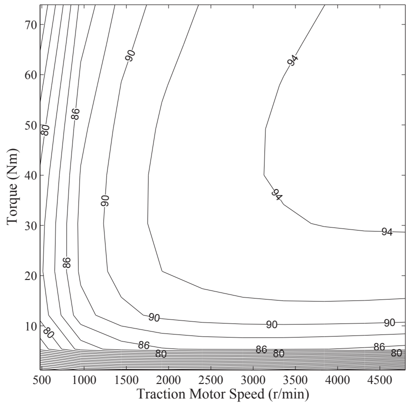

Fig. 9: RS motor efficiency map.

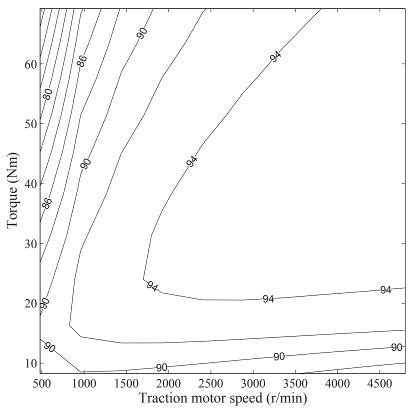

Fig. 10: FI-PM motor efficiency map.

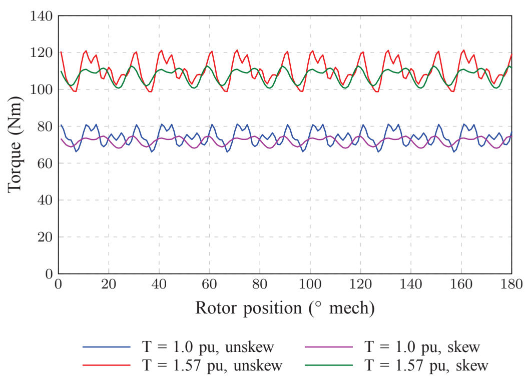

Fig. 11: RS motor torque versus rotor position.

VII. Measured Results

The RS motor, shown in Fig. 13, has been built and tested. The first set of tests consists of motor-to-dyno tests to determine if the motor performance correlates with the FE results. The second set of tests consists of motor-gearbox-to-dyno tests which represent the complete system, to determine the average gearbox efficiency of each gear.

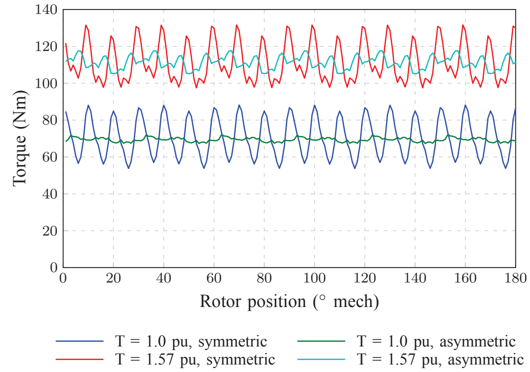

Fig. 12: FI-PM motor torque versus rotor position.

Fig. 13: RS motor.

A. Motor-to-Dyno Tests

The motor-to-dyno test setup consists of an inverter which drive the RS motor under test, which is connected to a eddy-current dynamo meter (dyno) via a torque transducer to measure shaft torque. The dyno is controlled by supplying DC current to its terminals. A photo of the experimental setup is shown in Fig. 14.

In Fig. 15 several simulated and measured torque values are plotted at different loads. Note that tests could only be done up to 2/3 of the rated load current and up to a maximum speed of 3000 r/min due to practical limitations.

From Fig. 15 it is evident that the measured and FE results compare very well. This is also true for the efficiency shown in Fig. 16 which is calculated and measured for the same loads as the torque.

B. Motor-Gearbox-Differential-to-Dyno Tests

The motor-gearbox-differential-to-dyno test setup consists of a inverter which drive the RS motor

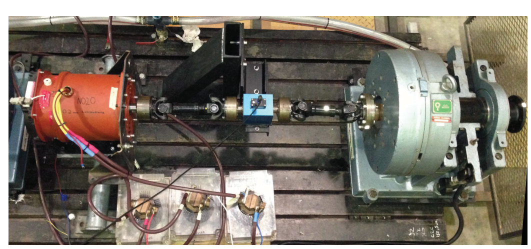

Fig. 14: Motor-to-Dyno test setup. From left to right is the RS motor (brown), torque transducer (blue) and dyno (grey-blue).

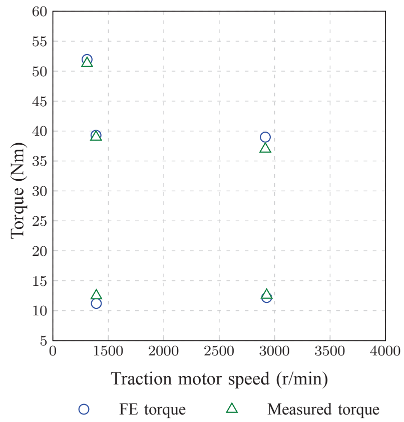

Fig. 15: Measured versus FE torque.

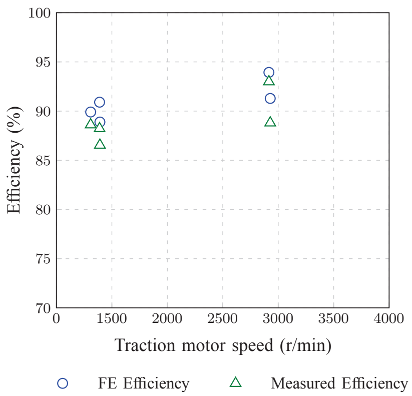

Fig. 16: Measured versus FE efficiency.

which is connected to the 5-speed manual gearbox and differential of the Opel Corsa, shown in Fig. 17, which is connected to two dyno's via the CV-joints as shown in Fig 18. Both dyno's have load cells to measure the wheel torque.In Tables V-VIII the gearbox efficiencies are given for 5^{th} - 2^{nd} gear at different loads. The gearbox efficiency includes the efficiency of the differential. The system efficiency excludes the efficiency of the inverter. Note that 1st gear is not tested

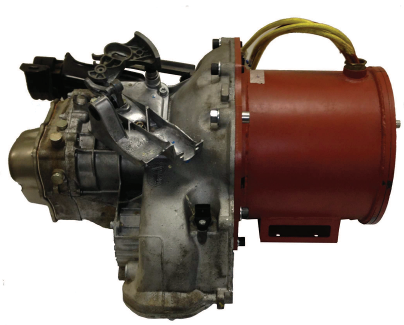

Fig. 17: RS motor together with the 5-speed manual gearbox and differential.

since the dyno must operate at higher speeds to be able to create high torque.

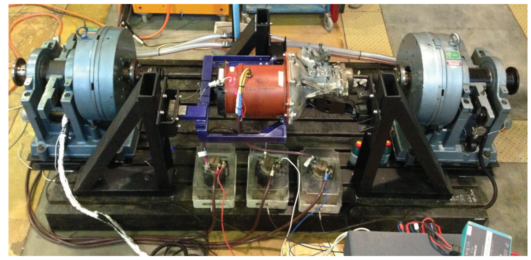

Fig. 18: Motor-gearbox-differential-to-dyno test setup.

TABLE V: Performance of the drive system in 5^{th} gear. Gear ratio 3.51448

f	P_{in}	T_{wheel}	η_{system}	η_{motor}	$\eta_{(gearbox+diff)}$
39.6	3.65	79.298	74.62	85.4	87.74
79	7.081	79.12	79.1	88.1	89.78
117.6	10.63	78.48	77.78	90.1	86.3

TABLE VI: Performance of the drive system in 4^{th} gear. Gear ratio 4.41674

f	P_{in}	T_{wheel}	η_{system}	η_{motor}	$\eta_{(gearbox+diff)}$
40.9	3.25	90.46	80.88	84.7	95.5
80.18	6.418	91.08	81.09	85.4	94.9
119.6	9.51	89.4	80.0	88.3	90.6

TABLE VII: Performance of the drive system in 3^{rd} gear. Gear ratio 5.57116

f	P_{in}	T_{wheel}	η_{system}	η_{motor}	$\eta_{(gearbox+diff)}$
39.9	3.471	126.9	82.3	89.3	92.16
81.85	6.977	125.63	82.97	90.2	91.9
119.5	10.483	127.6	81.9	91.6	89.4

TABLE VIII: Performance of the drive system in 2^{nd} gear. Gear ratio 8.416

f	P_{in}	T_{wheel}	η_{system}	η_{motor}	$\eta_{(gearbox+diff)}$
41.14	3.633	196.48	83.11	88.82	93.57
80.53	6.941	195.46	84.34	91.3	92.3
118.5	10.161	193.48	83.95	92.8	90.4

VIII. Flux Barrier-Rotor FI-PM Motor

Another FI-PM motor with rotor flux barriers was designed which is shown in Fig. 19. The focus for this motor was to reduce the stack volume of the motor, but still meet the specifications of the RS motor, thus, reducing magnet volume. The same stator cross-section is used as the RS and FI-PM motor.

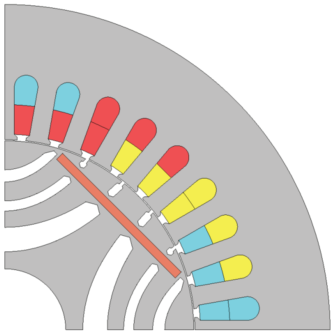

Fig. 19: Quarter cross-section of flux barrier-rotor FI-PM motor.

The optimum values for the design variables found through optimization are given in Table IX.

TABLE IX: Optimum design variables for flux barrier rotor FI-PM motor

Variables	δ	ℓ_s	b_{p1}	b_{p2}	b_{p3}
Values	85.81°	88.65	15.84°	25.87°	38.81°
Variables	b_{w1}	b_{w2}	b_{w3}		
Values	4.27	3.55	8.66		

Note that the stack length is a variable and the optimum is quite shorter (from 110 mm to 88.65 mm) than the stack length of the previous motors. The optimum current space phasor angle δ is much larger than that of the FI-PM motor therefore a increase in power factor. The performance parameters of this motor is given in Table X for rated torque and 4800 r/min. Note the 21 % decrease in magnet volume from the first FI-PM motor of Fig. 8.

Future work on the flux barrier rotor FI-PM motor is to lower the torque ripple by using an asymmetric flux barrier rotor FI-PM motor.

TABLE X: Performance of flux barrier rotor FI-PM Motor

Parameters	I_{rms}	V_{rms}	T	T_{ripple}
Values	$142.78A$	$117.05V$	$68.1N.m$	14.0%
Parameters	P_{cu}	P_{iron}	P_{rot}	P_{out}
Values	$1266W$	$292.73W$	$136.6W$	$34.1kW$
Parameters	η	P_f	CU_{mass}	PM_{volume}
Values	96.27%	0.86	$8.4kg$	$63.15cm^3$

IX. Conclusion

In the paper a variable-gear (VG) EV drive with either a RS or a FI-PM as traction motor is proposed and investigated. Both optimum designed motors are shown to perform very well considering the volumetric space available and the required torque and power specifications. The efficiencies found for both motors are well above 90% at high (maximum) operating frequency and at full flux. The high efficiency is due to, amongst other things, the relatively low core losses using high frequency stator lamination steel; the core losses are found to be approximately a third of the copper losses. The performance of the FI-PM motor with the same volume as the RS motor is surprising considering the simple FI-PM rotor structure. This simple rotor structure was designed for comparison reasons only, therefore the same volume as the RS motor were used. A new FI-PM motor was designed with a flux barrier-rotor. This rotor shows very good performance. The stack length reduced by 19%, while there were an increase in power factor and efficiency. The increase in power factor can be described to the increase in current space phasor angle while the increase in efficiency can be described by the reduced iron losses amongst other things. The flux barrier-rotor FI-PM also shows good saliency at full load which is favourable for sensorless control. The efficiency measured for the VG EV drive system excluding the inverter, i.e. from the motor through the gearbox to the differential output, is on average found to be above 80% for the different gear ratios, except for 5$^{\text{th}}$ gear where the efficiency is slightly lower than 80 %.

References

[1] M. Ehsani, Y. Gao, and A. Emadi, *Modern Electric, Hybrid Electric, and Fuel Cell Vehicles: Fundamentals, Theory, and Design*, 2nd ed. CRC Press, 2010.

[2] L. Lai and M. Ehsani, "Sensitivity analysis of vehicle performance to transmission parameters in parallel hevs with dynamic programming optimization," in *Transportation Electrification Conference and Expo (ITEC), 2012 IEEE*, June 2012, pp. 1 –5.

[3] Q. Ren, D. Crolla, and A. Morris, "Effect of transmission design on electric vehicle (ev) performance," in *Vehicle Power and Propulsion Conference, 2009. VPPC '09. IEEE*, sept. 2009, pp. 1260 –1265.

[4] S. Roberts, "Multi-speed transmissions for electric vehicle applications," *ATZ Worldwide*, vol. 114, no. 4, pp. 8–11, 2012.

[5] A. Sorniotti, M. Boscolo, A. Turner, and C. Cavallino, "Optimization of a multi-speed electric axle as a function of the electric motor properties," in *Vehicle Power and Propulsion Conference (VPPC), 2010 IEEE*, Sept. 2010, pp. 1 –6.

[6] T. Hofman and C. Dai, "Energy efficiency analysis and comparison of transmission technologies for an electric vehicle," in *Vehicle Power and Propulsion Conference (VPPC), 2010 IEEE*, Sept. 2010, pp. 1 –6.

[7] J. Germishuizen, F. Van der Merwe, K. Van der Westhuizen, and M. Kamper, "Performance comparison of reluctance synchronous and induction traction drives for electrical multiple units," in *Industry Applications Conference, 2000. Conference Record of the 2000 IEEE*, vol. 1, 2000, pp. 316–323 vol.1.

[8] A. Boglietti, A. Cavagnino, M. Pastorelli, and A. Vagati, "Experimental comparison of induction and synchronous reluctance motors performance," in *Industry Applications Conference, 2005. Fourtieth IAS Annual Meeting. Conference Record of the 2005*, vol. 1, 2005, pp. 474–479 Vol. 1.

[9] S. Wu, D. Reigosa, Y. Shibukawa, M. Leetmaa, R. Lorenz, and Y. Li, "Interior permanent-magnet synchronous motor design for improving self-sensing performance at very low speed," *Industry Applications, IEEE Transactions on*, vol. 45, no. 6, pp. 1939 –1946, Nov.-Dec. 2009.

[10] N. Limsuwan, Y. Shibukawa, D. Reigosa, and R. Lorenz, "Novel design of flux-intensifying interior permanent magnet synchronous machine suitable for self-sensing control at very low speed and power conversion," *Industry Applications, IEEE Transactions on*, vol. 47, no. 5, pp. 2004 –2012, Sept.-Oct. 2011.

[11] Y.-K. R. Chin and J. Soulard, "Modeling of iron losses in permanent magnet synchronous motors with field-weakening capability for electric vehicles," *International Journal of Automotive Technology*, vol. 4, no. 2, pp. 87–94, 2003, qC 20100901.

[12] V. der Plaats, *Numerical optimization techniques for engineering design*, V. Research and D. Incorporation, Eds. Mcgraw Hill, 2005, vol. 4th.